

The effects of unresolved double-degenerates in the white dwarf luminosity function

A. Rebassa-Mansergas^{1,2*}, S. Toonen³, S. Torres^{1,2} and P. Canals¹

¹ *Departament de Física, Universitat Politècnica de Catalunya, c/Esteve Terrades 5, 08860 Castelldefels, Spain*

² *Institut d'Estudis Espacials de Catalunya, Ed. Nexus-201, c/Gran Capità 2-4, 08034 Barcelona, Spain*

³ *School of Physics and Astronomy, University of Birmingham, Edgbaston, Birmingham B15 2TT, United Kingdom*

Accepted XXX. Received YYY; in original form ZZZ

ABSTRACT

We perform an analysis of the single white dwarf and the double degenerate binary populations in the solar neighbourhood following a population synthesis approach to investigate the effects of unresolved double degenerates in the white dwarf luminosity function. We consider all unresolved synthetic binaries to be associated with fictitious effective temperatures and surface gravities that are obtained in the same way as if these objects were observed as single point sources. We evaluate the effects of unresolved double white dwarfs assuming that the synthetic samples are “observed” both by the magnitude-limited SDSS and the volume-limited *Gaia* surveys, the latter limited to a distance of no more than 100 pc. We find that, for our standard model, the impact of unresolved double degenerates in the white dwarf luminosity function derived from the *Gaia* sample is nearly negligible. Unresolved double degenerates are hence expected to have no effect on the age of the Galactic disc, nor on the star formation history from this population. However, for the SDSS sample, the effect of unresolved double degenerates is significant at the brighter bins ($M_{\text{bol}} < 6.5$ mag), with the fraction of such systems reaching $\approx 40\%$ of the total white dwarf population at $M_{\text{bol}} = 6$ mag. This indicates unresolved double degenerates may influence the constraints on the star formation history derived from the SDSS white dwarf sample.

Key words: (stars:) white dwarfs – (stars:) binaries (including multiple): close – stars: luminosity function, mass function

1 INTRODUCTION

It is well established that white dwarfs (WDs) are the remnants of main sequence stars of masses up to $\approx 8 - 11 M_{\odot}$ (e.g. Siess 2007). Thus, WDs are by far the most common end product of stellar evolution. WDs are supported by the pressure of the degenerate electrons in their interiors and are subject to a relatively well understood cooling process that drives their evolution (e.g. Althaus et al. 2010; Renedo et al. 2010; Tremblay et al. 2011; Camisassa et al. 2016). The theoretical cooling sequences allow deriving accurate WD cooling ages from the observationally determined effective temperatures and surfaces gravities. By making use of an initial-to-final mass relation (e.g. Andrews et al. 2015; Cummings et al. 2018) and adopting a metallicity value, one can also derive the WD progenitor masses and their lifetimes from the appropriate main sequence evolutionary sequences (e.g. BaSTI; Pietrinferni et al. 2004). This yields the total WD ages by simply adding the cooling times to

the main sequence progenitor lifetimes. Hence, WDs have been used as reliable cosmochronometers for the determination of ages. Some relevant examples of using WDs as cosmochronometers include constraining the age-metallicity relation of the Galactic disk (Rebassa-Mansergas et al. 2016), the age-rotation-activity relation of low-mass main sequence stars (Rebassa-Mansergas et al. 2013; Skinner et al. 2017) or the age-velocity dispersion relation of the Galactic disk (Anguiano et al. 2017). It has to be emphasised however that the most efficient way of using WDs as reliable age indicators is via the study of the WD luminosity function.

The WD luminosity function is defined as the number of WDs per cubic parsec as a function of unit luminosity (see García-Berro & Oswalt 2016 for a recent review). In particular, the analysis of the WD luminosity function has provided age estimates for the different components of the Galactic disk (Winget et al. 1987; Garcia-Berro et al. 1988; Fontaine et al. 2001; Torres & García-Berro 2016; Kilic et al. 2017), constrained the local star formation rate (Diaz-Pinto et al. 1994; Rowell 2013; Isern 2019) and provided the ages of both open and globular clusters (e.g.

* E-mail: alberto.rebassa@upc.edu

García-Berro et al. 2010; Jeffery et al. 2011; Hansen et al. 2013; Torres et al. 2015). However, it is important to note that the observed samples from which the WD luminosity functions are constructed suffer from several drawbacks, which requires addressing the following issues (García-Berro & Oswalt 2016):

- An ultra large WD sample is needed, of the order of 10^5 stars, to map the luminosity function with the smallest luminosity bins as possible.
- Precise parallaxes and proper motions are required, substantially better than 1 mas and 1 mas/yr, respectively. This is necessary for the identification of WD components of the different Galactic disks and the halo. For example, the precise parallaxes and proper motion measurements obtained by the *Gaia* mission have permitted to classify the different Galactic components in a volume-limited sample (Torres et al. 2019a).
- Spectroscopic identifications of sufficient resolution for velocity determinations are mandatory, not only for cataloguing the stars as members of the different components, but also for kinematic studies that identify Galactic structures (Torres et al. 2019b).
- Improved atmospheric models for very cool WDs are desired for a proper determination of their stellar parameters.
- Better categorization and treatment of selection effects are needed to account for all possible observational biases affecting the samples.
- Quantifying the effects of unresolved binaries is needed to understand to what extent the luminosity function is contaminated.

Fortunately, the first two issues are being addressed by the *Gaia* mission (Gaia Collaboration et al. 2016), which is providing unprecedented samples of WDs, both magnitude- (Gentile Fusillo et al. 2019, over 250,000 objects) and volume-limited (Hollands et al. 2018; Jiménez-Esteban et al. 2018), along with very accurate photometry and astrometry. Moreover, WD radial velocities of uncertainties ≈ 10 km/s can be determined from medium resolution spectroscopy if the signal-to-noise ratio is sufficiently high (see, for example, Anguiano et al. 2017). We are also improving our understanding of atmospheric models for cool WDs (Blouin et al. 2019; Tremblay et al. 2019) as well as WD evolutionary sequences (Camisassa et al. 2016, 2018; De Gerónimo et al. 2018). With these improvements it is now possible to efficiently characterise most observational selection effects (e.g. Rebassa-Mansergas et al. 2015a; Cojocaru et al. 2017). However, the effects of unresolved binaries such as double degenerates in the WD luminosity function have not been yet explored in full detail. This is the aim of the presented work.

We study the effects of unresolved double degenerates in the WD luminosity function by means of a population synthesis simulator of the single WD and the double degenerate populations in the solar neighbourhood. We consider the synthetic samples as if they would have been observed by the magnitude-limited Sloan Digital Sky Survey (SDSS; York et al. 2000; Stoughton et al. 2002) and the *Gaia* mission, which provides a volume-limited WD sample for distances up to 100 pc (Jiménez-Esteban et al. 2018).

2 THE POPULATION SYNTHESIS CODE

We used the population synthesis code *SeBa* (Portegies Zwart & Verbunt 1996; Toonen et al. 2012) to generate synthetic populations of single and double WDs. In both cases we only considered hydrogen-rich (DA) atmospheres, which are by far the most common spectral types among WDs (Kepler et al. 2019). We followed the evolution of the stars from the zero-age main-sequence to the current epoch. The double degenerate populations were those we used in Rebassa-Mansergas et al. (2019). For a full description of the model, we refer the reader to Rebassa-Mansergas et al. (2019), whilst a full review of the population synthesis method used here can be found in Toonen et al. (2014).

For the initial population of single stars, we assumed that their masses followed the initial mass function of Kroupa et al. (1993) with a range between 0.1 - $100M_{\odot}$. Based on the same population synthesis approach, 10-30% of single WDs may form through binary system mergers (Toonen et al. 2017; Temmink et al. 2019). Other studies claim fractions of $\approx 10\%$ (Maoz et al. 2018) and $\approx 15\%$ (Kilic et al. 2018). The impact of such mergers in the WD luminosity function will be studied in a future publication. Hence, single WDs that result from binary system mergers were not taken into account in this work. The initial mass function was also adopted for deriving the initial masses of the initially most massive star in the binary. The masses of the companion stars were drawn from a uniform distribution in the mass ratio between 0 and 1 (Raghavan et al. 2010; Duchêne & Kraus 2013; De Rosa et al. 2014; Cojocaru et al. 2017). The lowest value used for the mass ratio was 1×10^{-10} . The orbital separation followed a uniform logarithmic distribution (Abt 1983), and the eccentricity a thermal distribution (Heggie 1975). We adopted a constant binary fraction of 50% as is appropriate for A-, F-, and G-type stars (Raghavan et al. 2010; Duchêne & Kraus 2013; Moe & Di Stefano 2017; De Rosa et al. 2014) and solar metallicities.

The formation of double WDs was determined by the common-envelope (CE) phase. This is a short phase in the evolution of the system, in which both stars share a single (that is common) envelope (see Ivanova et al. 2013, for a comprehensive review). It plays an important role in the formation of many compact binaries, as the orbit is expected to shrink due to friction. The CE-phase is poorly understood, and therefore we applied two different models, designated by $\alpha\alpha$ and $\gamma\alpha$. In the former, the modelling of the CE-phase was based on the energy budget (Paczynski 1976; Tutukov & Yungelson 1979; Webbink 1984; Livio & Soker 1988):

$$\alpha\Delta E_{\text{orb}} = E_{\text{gr}} \equiv \frac{GM_{\text{env}}}{\lambda R}, \quad (1)$$

where α is the efficiency with which orbital energy E_{orb} is consumed to unbind the CE with binding energy E_{gr} , M the mass of the donor star, M_{env} the envelope mass, λ the binding energy parameter that depends on the structure of the primary star, and R the radius of the donor star. We adopted $\alpha\lambda = 2$ based on the reconstruction of the last phase of mass transfer in the evolution of observed double WDs, as in Nelemans et al. (2000).

In our other model ($\gamma\alpha$), we adopted an alternative prescription for the CE-phase if the binary did not contain any compact object and the system was stable against the Darwin-Riemann instability (Darwin 1879). In this alternative model, the angular-momentum budget was considered:

$$\frac{\Delta J}{J_{\text{init}}} = \gamma \frac{\Delta M}{M + m}, \quad (2)$$

where J is the angular momentum of the binary, m the mass of the companion, and γ the efficiency with which angular momentum is used to unbind the envelope. The model is also inspired by the work of Nelemans et al. (2000). Here we adopted $\gamma = 1.75$, as in Nelemans et al. (2001a).

We assumed a star formation history (SFH) appropriate for the Milky Way that is dependent on Galactocentric radius and time following Boissier & Prantzos (1999) (see Toonen & Nelemans 2013 for a full description of the model). The absolute magnitudes of the WDs were obtained from the cooling sequences of pure hydrogen-rich atmospheres (i.e. DA WDs) from Holberg & Bergeron (2006), Kowalski & Saumon (2006) and Tremblay et al. (2011)¹. The absolute magnitude of a WD was converted into apparent magnitude using its distance (as provided by the SFH model) and the interstellar extinction based on its location in the Galaxy (see Toonen & Nelemans 2013).

3 UNRESOLVED DOUBLE-DEGENERATES

The population synthesis code described in the previous Section provided two different WD populations, namely the single WD sample and the double-degenerate population. Among the double-degenerate binaries, we were specially interested in unresolved pairs, since they are observed as “single” WDs. The stellar parameters observationally derived from the combined fluxes of these unresolved double-degenerates are not real (they could be considered as good approximations for the hotter and/or less massive WD if it were much more luminous than the companion). Hence, the inclusion of these apparently single WDs contaminates the luminosity function. In order to analyse the level of contamination, it became necessary to derive the luminosities (or bolometric magnitudes in our case) for the unresolved double-degenerates as they would have been obtained from observations. We did this as follows.

The first step was to evaluate which synthetic double-degenerates can be considered as unresolved. To that end, we calculated the angular separation of each binary using equation 12 of Toonen et al. (2017). As we have already mentioned, we focus our study on the WD populations as they would have been observed by the SDSS and the *Gaia* surveys. We thus considered as unresolved double-degenerates those binaries with angular separation of 1” or less for the SDSS sample (York et al. 2000), and of 0.5” or less for the *Gaia* sample (de Bruijne et al. 2015). Once the unresolved binaries were identified, we obtained their synthetic spectra (resulting from summing up the individual WD fluxes) following the method described in Rebassa-Mansergas et al.

(2019). In summary, the spectra of the individual components were obtained interpolating the corresponding effective temperature and surface gravity values on an updated grid of model atmosphere spectra of Koester (2010), which incorporates model spectra down to effective temperatures of 4000 K. The resulting combined synthetic spectra were then fitted with the same grid of hydrogen-rich WD model atmosphere spectra to derive the fictitious effective temperatures and surface gravities (for details see Rebassa-Mansergas et al. 2017). These values were then interpolated in the WD cooling sequences of Renedo et al. (2010) for deriving the bolometric magnitudes. In cases where the individual components were both below 5000 K we could not trust the surface gravity values derived from the fits since no Balmer lines were present in the spectra. Thus we derived a fictitious M_g absolute magnitude from the combined g apparent magnitude of the double degenerate and its distance (taking extinction into account), which together with the effective temperature (reliable from the fit) provided the bolometric magnitudes by interpolating in the cooling sequences mentioned above. We emphasise that the bolometric magnitude values derived here were obtained by considering the unresolved double-degenerates as single WDs and are therefore fictitious.

4 THE WHITE DWARF LUMINOSITY FUNCTION

We followed two different approaches to evaluate the impact of unresolved double-degenerates in the WD luminosity function. First, we considered the synthetic populations of single WD and double-degenerate binaries as they would have been observed by the SDSS magnitude-limited survey, which so far contains the largest number of spectroscopically confirmed WDs (for the latest updated catalogue see Kepler et al. 2019) from which several luminosity functions have been derived (Hu et al. 2007; De Gennaro et al. 2008; Rebassa-Mansergas et al. 2015b). The second approach was to only take into account synthetic WDs nearer than 100 pc, since these are accessible by the *Gaia* satellite and can be considered to be members of a volume-limited sample (Jiménez-Esteban et al. 2018). In both exercises we considered the unresolved synthetic WDs as single point sources of fictitious stellar parameters and bolometric magnitudes (Section 3).

4.1 The SDSS magnitude-limited sample

The SDSS is a magnitude-limited survey originally aimed at obtaining spectra of quasars and galaxies (York et al. 2000; Stoughton et al. 2002). The target selection algorithm was slightly modified during subsequent data releases (Yanny et al. 2009; SDSS-III Collaboration et al. 2012; Alam et al. 2015). This implies the spectroscopic catalogue of SDSS WDs is heavily affected by selection effects, despite the fact that it is the largest spectroscopic WD sample to date. The 14th data release (DR14) of SDSS compiles over 35,000 spectroscopically-identified WDs, the majority of which are of spectral type DA (hydrogen-rich atmospheres) with effective temperatures between ≈ 6000 K and $\approx 100,000$ K (Kepler et al. 2019).

¹ See also <http://www.astro.umontreal.ca/bergeron/CoolingModels>.

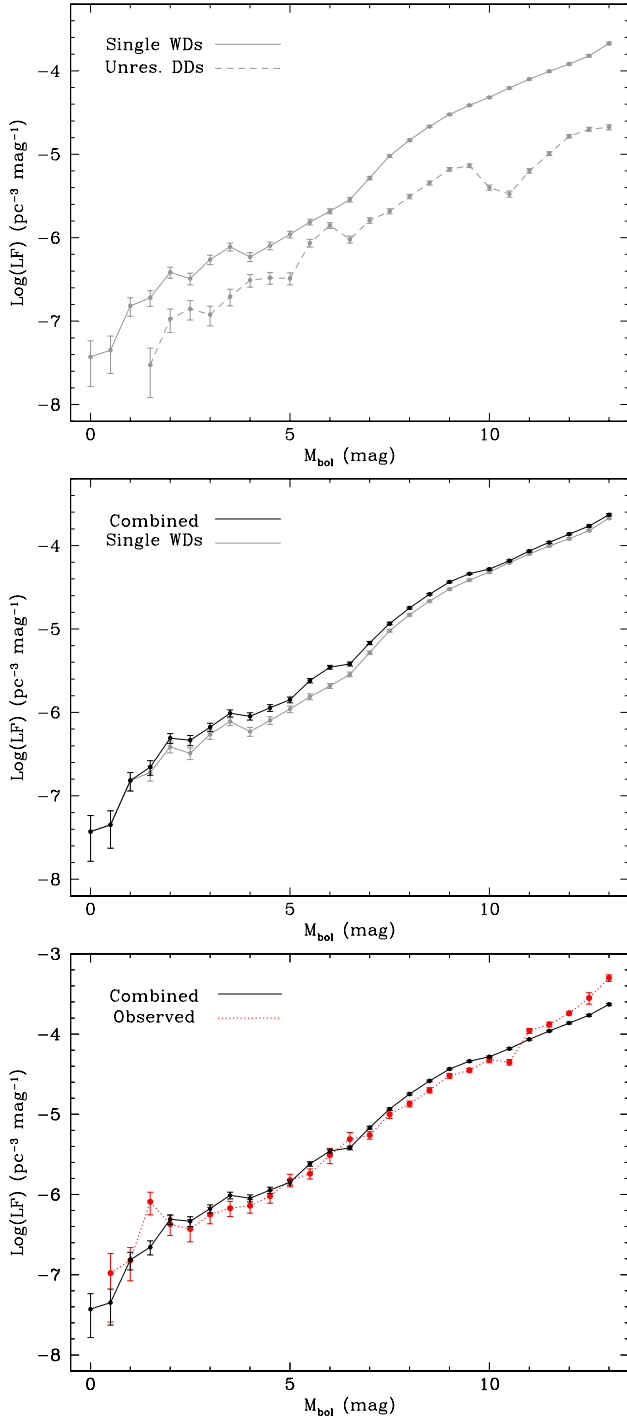


Figure 1. Top panel: the synthetic SDSS luminosity functions for the single WD (solid grey line) and the unresolved double degenerate (dashed grey line) samples obtained from our standard model. Middle panel: the combined luminosity function (single WD plus unresolved double degenerates; black solid line) as compared to the one derived from the single synthetic SDSS WD sample (grey solid line) when adopting our standard model. Bottom panel: the synthetic combined luminosity function resulting from assuming our standard model (black solid line) and the observed SDSS DA WD luminosity function (red dotted line; Rebassa-Mansergas et al. 2015b).

Here we analyse our synthetic single and binary WD samples as if they were observed by the SDSS survey with the ultimate goal of deriving the corresponding luminosity functions. As mentioned in Section 3, for the binary samples we calculated the angular separation of each source and filtered out all systems with an angle larger than $1''$, i.e. resolved binaries by the SDSS survey. We calculated the magnitudes of the unresolved binaries from the individual magnitudes of each binary component, taking interstellar extinction into account. Moreover, we only considered those synthetic WDs that fall within the DR14 spectroscopic plates (assuming a field of view of 7 deg^2 for each plate) and satisfying $14 \leq g \leq 19.1 \text{ mag}$. $g = 14 \text{ mag}$ is the lower magnitude limit of SDSS. The upper limit $g = 19.1 \text{ mag}$ was set due to the fact that fainter objects are generally associated with noisy SDSS spectra that were not used in the observed analysis of the SDSS luminosity function (see, for example, Rebassa-Mansergas et al. 2015b). Moreover, we excluded WDs of bolometric magnitudes fainter than $M_{\text{bol}} = 13 \text{ mag}$, since these objects are not present in the observed SDSS DA WD luminosity function (Rebassa-Mansergas et al. 2015b). Finally, we applied the photometric cuts in the SDSS filters for spectroscopic DA WDs provided by Girven et al. (2011). Thus, we obtained final synthetic double degenerates that evolved adopting the $\gamma\alpha$ formalism for common envelope and 4,674 unresolved WD binaries that evolved following the $\alpha\alpha$ formalism.

In order to account for the selection effects of a magnitude-limited sample, we applied a volume correction following the $1/V_{\text{max}}$ method (Schmidt 1968; Green 1980). This method calculates the maximum volume V_{WD} in which each synthetic WD would have been detected within the magnitude limits of the SDSS survey:

$$\begin{aligned}
 V_{\text{WD}} &= V_{\text{max}} - V_{\text{min}} = \sum_{i=1}^{n_{\text{plate}}} \frac{\omega_i}{4\pi} \int_{d_{\text{min}}}^{d_{\text{max}}} e^{-z/z_0} 4\pi r^2 dr = \\
 &= - \sum_{i=1}^{n_{\text{plate}}} \frac{z_0 \times \omega_i}{|\sin b|} \left[\left(r^2 + \frac{2z_0}{|\sin b|} r + \frac{2z_0^2}{|\sin b|^2} \right) e^{-\frac{r|\sin b|}{z_0}} \right]_{d_{\text{min}}}^{d_{\text{max}}} \quad (3)
 \end{aligned}$$

where b the Galactic latitude of the synthetic WDs and ω_i the solid angle (in steradians) covered by each SDSS DR14 plate. The quantity e^{-z/z_0} is essential to consider the non-uniform distribution of stars in the direction perpendicular to the Galactic disc, where $z = r \times \sin(b)$ the WD's distance from the Galactic plane and $z_0 = 200 \text{ pc}$ the scale height (Torres et al. 2019a). The lower/upper g magnitude limits of each SDSS plate define the minimum/maximum distance, d_{min} and d_{max} , at which an object belongs to the survey, hence the minimum/maximum volumes, $V_{\text{min}}/V_{\text{max}}$, where $V_{\text{WD}} = V_{\text{max}} - V_{\text{min}}$. The limits correspond to the minimum/maximum g magnitudes among all spectroscopic sources observed by each plate (Rebassa-Mansergas et al. 2015b). The upper limits were set to a maximum of 19.1 mag due to the fact that we restricted our WD synthetic samples to objects of g magnitudes brighter than this value.

As previously mentioned, the target selection algorithm of SDSS favoured the detection of hot WDs of similar colours to those of quasars. Therefore, the probability that a spectrum was obtained for a given WD and

contributes to the WD luminosity function depends on its colour. [Rebassa-Mansergas et al. \(2015b\)](#) applied a spectroscopic completeness correction to the SDSS DA WD observed sample to account for this observational bias. This implied the observed sample could be considered as spectroscopically complete. Therefore, rather than computing a detection probability for each of our synthetic WDs and applying the corresponding spectroscopic completeness correction, we assumed that all synthetic WDs falling within the field of view of the SDSS DR14 plates had an associated spectrum. In other words, our synthetic samples were also spectroscopically complete.

The synthetic single and double WD luminosity functions obtained using our adopted model (Section 2), hereafter our *standard model*, are illustrated in the top panel of Figure 1. We show the luminosity function from the $\gamma\alpha$ unresolved double WD population since this formalism best reproduces the observational data ([Nelemans et al. 2001b](#); [Toonen et al. 2012](#)). In both cases, the uncertainties are calculated following [Boyle \(1989\)](#). The functions display the expected monotonous increase in the number of systems with fainter bolometric magnitudes.

In the middle panel of Figure 1 we show the luminosity function resulting from combining the single plus unresolved double WD samples, which is compared to the single WD luminosity function. The contribution of unresolved double WDs is more pronounced at the brighter bins, especially between $\approx 4 \text{ mag} < M_{\text{bol}} < \approx 6 \text{ mag}$. Previous studies suggest that low-mass, helium-core WDs that are presumably in binary systems are the cause for an increase in the WD luminosity function below $M_{\text{bol}} = 4 \text{ mag}$ ([Krzyszinski et al. 2009](#); [Torres et al. 2014](#)), which seems to be in line with our results. The other bins of the luminosity function are scarcely contaminated by the presence of unresolved double degenerates. This can also be seen in the top panel of Figure 2, where we show the ratio of the space density of single WDs and the space density of unresolved double degenerates. The minimum fraction value (≈ 1.5) is achieved at $M_{\text{bol}} = 6 \text{ mag}$. In other words, unresolved double degenerates can represent, at most, $\approx 40\%$ of the objects with M_{bol} around 6 mag. It is also interesting to note that the ratio of the space density increases considerably at $M_{\text{bol}} \approx 10.5 \text{ mag}$, thus implying a drop in the space density of unresolved double degenerates. We need to recall here that the derived M_{bol} values for such binaries are fictitious and are not directly linked to real physical quantities. Moreover, unresolved system are short period binaries whose evolution followed at least two episodes of mass transfer. This implies that the mass distributions and formation times of these objects, and hence their M_{bol} distributions, are not expected to follow the distributions of both single WDs and WDs in resolved binaries.

The observed SDSS luminosity function derived by [Rebassa-Mansergas et al. \(2015b\)](#); this sample includes 5,857 apparently single DA WDs from the SDSS DR10 catalogue with $g \leq 19 \text{ mag}$ and with spectroscopic completeness correction values available) is illustrated in the bottom panel of Figure 1 (red dotted line). The increase in the observed space density at $M_{\text{bol}} = 2 \text{ mag}$ is very likely a consequence of having very few WDs at those bins, i.e. we suffer from low-number statistics. The cut at $M_{\text{bol}} = 13 \text{ mag}$ is due to the fact that the lower effective temperature value

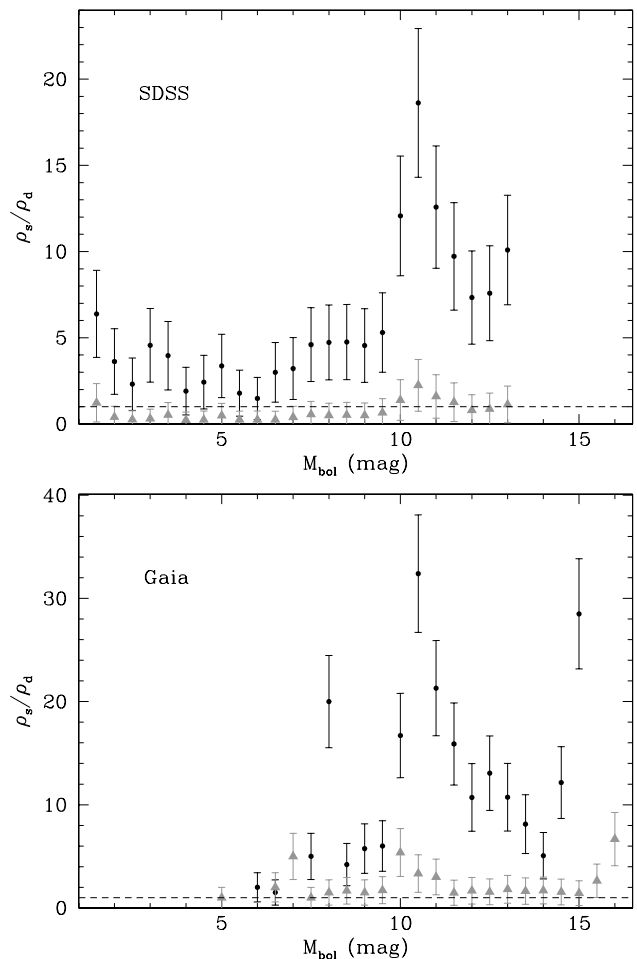


Figure 2. Top panel: the fraction between the space densities of single WDs and unresolved double degenerates in the synthetic SDSS sample for our standard model (black) and for the model producing the highest fraction of unresolved double degenerates (gray; see Section 5.1). Bottom panel: the same but for the *Gaia* synthetic samples. The horizontal dashed lines indicate fractions equal to 1.

that can be determined for a spectroscopic SDSS DA WDs is $\approx 6000 \text{ K}$. Superimposed to the observed SDSS luminosity function we display the one obtained from combining our single WD plus the unresolved double-degenerate synthetic samples. The combined function is a good match to the observed one except at the fainter bins ($M_{\text{bol}} = 12, 13 \text{ mag}$) where our simulations seem to under-predict the WD space density. Despite this discrepancy, our model assumptions seem to perform a good job at reproducing the the WD and WD binary populations in the solar neighbourhood. Therefore, under the assumptions of our standard model, the contribution of unresolved double degenerates appears to be important only at the brighter bins. The extra contribution of apparently single WDs in the luminosity function in these bins ($M_{\text{bol}} < 6.5 \text{ mag}$) is expected to affect the derived star formation history from observed SDSS WD samples (e.g. [Hu et al. 2007](#)). A typical $0.6 M_{\odot}$ WD with $M_{\text{bol}} = 6 \text{ mag}$ (where we have the highest contamination) has a total age of around 1.5 Gyr ([Camisassa et al. 2016](#)). This implies that a 40% contamination (we take the maximum possible value)

in the WD luminosity function for $M_{\text{bol}} < 6.5$ mag translates into a 40% uncertainty in the derived SFR for ages younger than 1.5 Gyr.

The luminosity functions obtained when adopting the $\alpha\alpha$ unresolved double degenerate sample were nearly identical to those shown in Figure 1 for the $\gamma\alpha$ samples. This indicates the common envelope formalism adopted plays no important role in shaping the luminosity function. Note that modifying the particular values of the CE efficiency α for the $\alpha\alpha$ formalism and the γ efficiency for the $\gamma\alpha$ prescription do change the fraction of resulting unresolved double degenerates². However, the assumed values in our standard model are already providing the highest possible fractions, so altering these values will only result in a lower fraction of double WDs and hence an even lower impact in the WD luminosity function.

4.2 The *Gaia* 100 pc volume-limited sample

Thanks to the data provided by the *Gaia* mission we now have at hand the largest sample of WDs ever obtained, which includes over 250 000 objects (Gentile Fusillo et al. 2019). Jiménez-Esteban et al. (2018) demonstrated that the *Gaia* WD sample can be considered as a volume-limited one for distances up to 100 pc from the Sun. This implies one can directly obtain the WD luminosity function without the need of applying a volume correction, i.e. without the need of applying the $1/V_{\text{max}}$ method. This of course requires deriving the bolometric luminosities of the WDs, which currently can only be obtained photometrically since most of the *Gaia* WDs have no spectra yet. However, this exercise is subject to large uncertainties due to the fact that we do not know the spectral types of the WDs, hence the need of adopting, as a first approximation, those for hydrogen-rich WDs.

In this section we evaluate the impact of unresolved double degenerates in the *Gaia* WD luminosity function that will eventually be obtained once all *Gaia* WDs have been spectroscopically observed.

To derive the corresponding luminosity functions we considered single WDs and unresolved double degenerates of effective temperatures (fictitious values for the latter sample) down to 4000 K and with distances within 100 pc. The chosen lower effective temperature limit was not of much concern since the Galaxy is not old enough to have generated many WDs cooler than this. Indeed, cooler WDs are very seldom observed in current volume-limited samples (e.g. the 40 pc sample from Limoges et al. 2015). As previously mentioned, we considered as unresolved binaries those with angular separations less than 0.5". In this case, the number of synthetic single WDs was 13,865 and the number of unresolved double WDs for the $\gamma\alpha$ and $\alpha\alpha$ samples were 1017 and 670, respectively.

² The fraction of double WDs amongst single WDs differs by a factor of about 2 between the two different models, with the $\gamma\alpha$ formalism proving the larger number of double WDs (Rebassa-Mansergas et al. 2019). Unfortunately, the difference between the observationally derived fractions is larger, which implies we cannot use them yet to constrain binary evolution. Toonen et al. (2017) (using the same models) discuss the prospects for this with the upcoming large and homogeneously selected samples from *Gaia*.

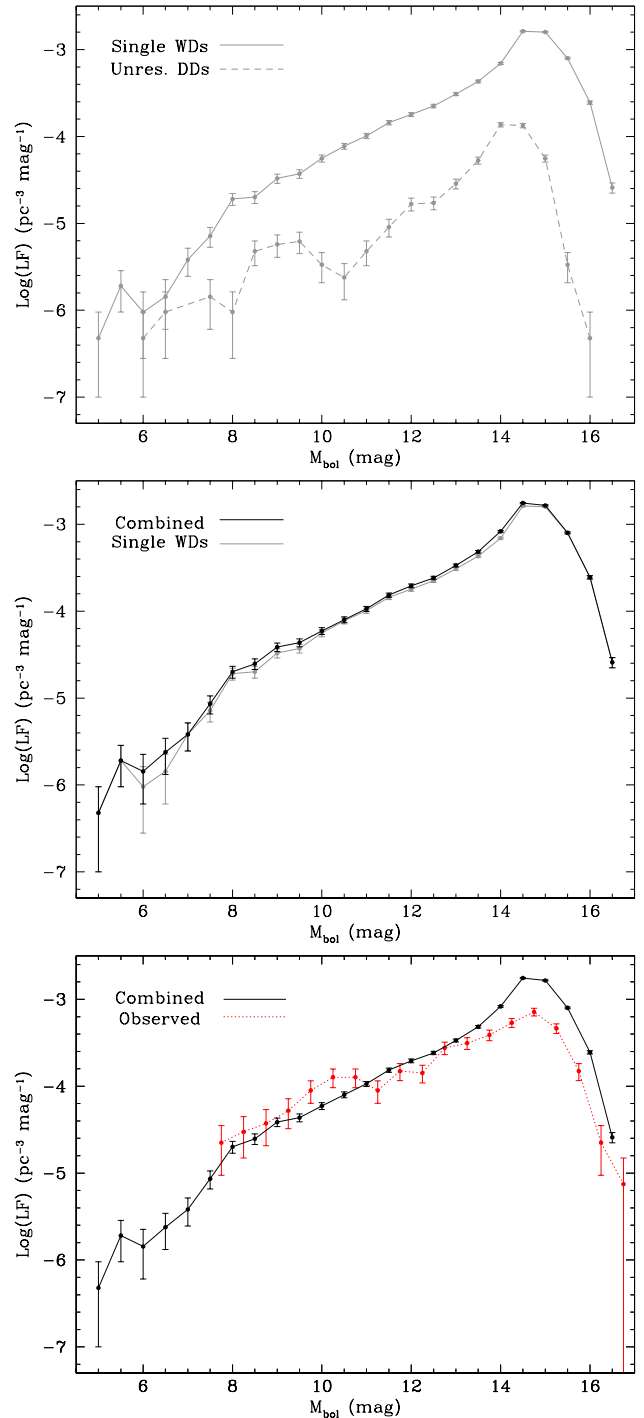


Figure 3. The same as Figure 1 but for the *Gaia* samples. The red dotted line in the bottom panel corresponds to the observed luminosity function of Limoges et al. (2015) for DA WDs within 40 pc of the Sun.

The synthetic functions are shown in the top panel of Figure 3, where the errors are calculated assuming Poisson statistics. For the same reason as for the SDSS sample, we only display the $\gamma\alpha$ double WD binary population. In both cases, the number of WDs increases for fainter bolometric magnitude bins until we reach $M_{\text{bol}} \approx 15$ mag. From then on, the space densities decrease sharply, as expected from the

finite age of the Galactic disk in a volume-limited survey. It is worth noting that the very bright M_{bol} bins (<5 mag) are absent of WDs due to the relatively small volume sample we are considering (100 pc), i.e. the larger the volume the more likely it is to detect very hot WDs. The ratio of the space densities vs. M_{bol} for single WDs and unresolved double degenerates is illustrated in the bottom panel of Figure 2. It becomes obvious that the number of unresolved double WDs is much smaller in the *Gaia* sample than in the SDSS sample, a simple consequence of the fact that the angular separation of the binaries that the *Gaia* survey can resolve is half the SDSS one. Therefore, the impact of unresolved double degenerates in the single WD luminosity function is nearly negligible (see middle panel of Figure 3). The only region where there are slight differences between the luminosity functions for single WDs and the combined sample is near $M_{\text{bol}} = 6$ mag (similar to the result obtained using the SDSS sample; Figure 1). Even here, the discrepancies in the *Gaia* case are within the expected errors and can therefore not be considered as significant. Also worth noting is that the ratio of the space densities for single WDs and unresolved double degenerates increases considerably at $M_{\text{bol}} \approx 10.5$ mag (bottom panel of Figure 2). This increase is related to a drop in the space density of unresolved double degenerates, an effect that was also observed in our SDSS sample (top panel of Figure 2). The fact that both the SDSS and *Gaia* samples display the same effect rules out the possibility that the drop in space density of unresolved double WDs at those bins is a consequence of selection effects, since the *Gaia* sample is volume-limited.

For completeness, the bottom panel of Figure 3 displays the synthetic combined luminosity function and the observed function from Limoges et al. (2015) for WDs within 40 pc of the Sun (from this sample we only considered DA WDs that are not part of resolved binaries). The agreement between the two functions is reasonable considering the observational errors except for $M_{\text{bol}} > 14$ mag, where the synthetic function clearly over-predicts the observed one. This could be related to the fact that our standard model assumes solar metallicities rather than a dispersion in metallicities around the solar value (Tononi et al. 2019).

In the same way as for the SDSS sample, the luminosity functions obtained by adopting the $\alpha\alpha$ unresolved double degenerate sample were nearly identical to those derived from the $\gamma\alpha$ samples.

We conclude that, under the assumptions of our standard model, the star formation history and the age of the Galactic components that will be eventually derived from the *Gaia* 100 pc sample will not be affected by the presence of unresolved double degenerates in the WD luminosity function.

5 DISCUSSION

We have adopted a standard model based on several assumptions that best agree with observational data to reproduce the population of unresolved double degenerates (Section 2) and to evaluate their impact in the WD luminosity function (Section 4). However, the resulting fraction of unresolved double WDs clearly depends on these assumptions (e.g. Claeys et al. 2014). Therefore, there may exist other

models that yield a higher number of unresolved double degenerates. Moreover, resolved double WDs have so far not been taken into account in our analysis despite the fact that, observationally speaking, the binary components would be considered as single WDs and hence also contribute to some extent to the WD luminosity function. Finally, we have also neglected the contribution from WDs that are part of binaries with main sequence companions. In this section we discuss the impact of these issues.

5.1 The fraction of unresolved double degenerates

We performed a new simulation to investigate to what extent the highest expected fraction of unresolved double WDs contaminates the WD luminosity function. To that end, we modified two assumptions in our standard model: (1) the binary fraction was increased from 50% to 85% and (2) a mass ratio distribution of the form $n(q) \propto q$ was adopted, where q is the ratio of the secondary and primary masses, instead of a uniform mass ratio distribution. The two modifications were based on a Monte Carlo simulator study that compares the fraction of synthetic resolved WD binaries to the observed fraction and allows for deviations between the computed and the observed values up to one order of magnitude (Canals et al., in prep.). The first assumption increased the number of initial main sequence binaries and therefore the number of resulting double WDs. The second implied that it was more likely to form binaries of similar component masses, which favoured the secondary stars to be more massive and hence to be able to evolve out of the main sequence within the Hubble time, thus producing a larger number of close double WDs. The number of unresolved double degenerates we obtained using this model was approximately double that of our standard model. We derived the corresponding SDSS and *Gaia* luminosity functions in the same way as described above for our standard model. The functions are illustrated in Figures 4 and 5 for the SDSS and *Gaia* sample, respectively. The ratio of the space densities of single WDs to unresolved double degenerates obtained with this new model is illustrated in grey in Figure 2.

Because of the high binary fraction assumed, the space density of single SDSS WDs was lower than the one derived for the unresolved double degenerate binaries for most M_{bol} bins (see the top panel of Figure 4 and top panel of Figure 2). As a consequence, the synthetic SDSS WD luminosity function is clearly affected by the inclusion of this extra number of double degenerates (see the middle panel of Figure 4). If this was a valid model, then the star formation rate derived from the SDSS luminosity function should be taken with extreme caution due to the large contamination from unresolved double degenerates. However, the total synthetic space density (single WDs plus unresolved double degenerated) clearly underestimates the space density for the observed SDSS WDs at the bright ($M_{\text{bol}} < 2$ mag) and faint ($M_{\text{bol}} > 9$ mag) bins (see the bottom panel of Figure 4). This suggests the high number of unresolved double degenerates predicted by this model is unrealistic, most likely because the adopted assumptions, as compared to our standard model, are less supported by the observational data.

As expected, the number of unresolved double degenerates also increased in the *Gaia* synthetic sample. However,

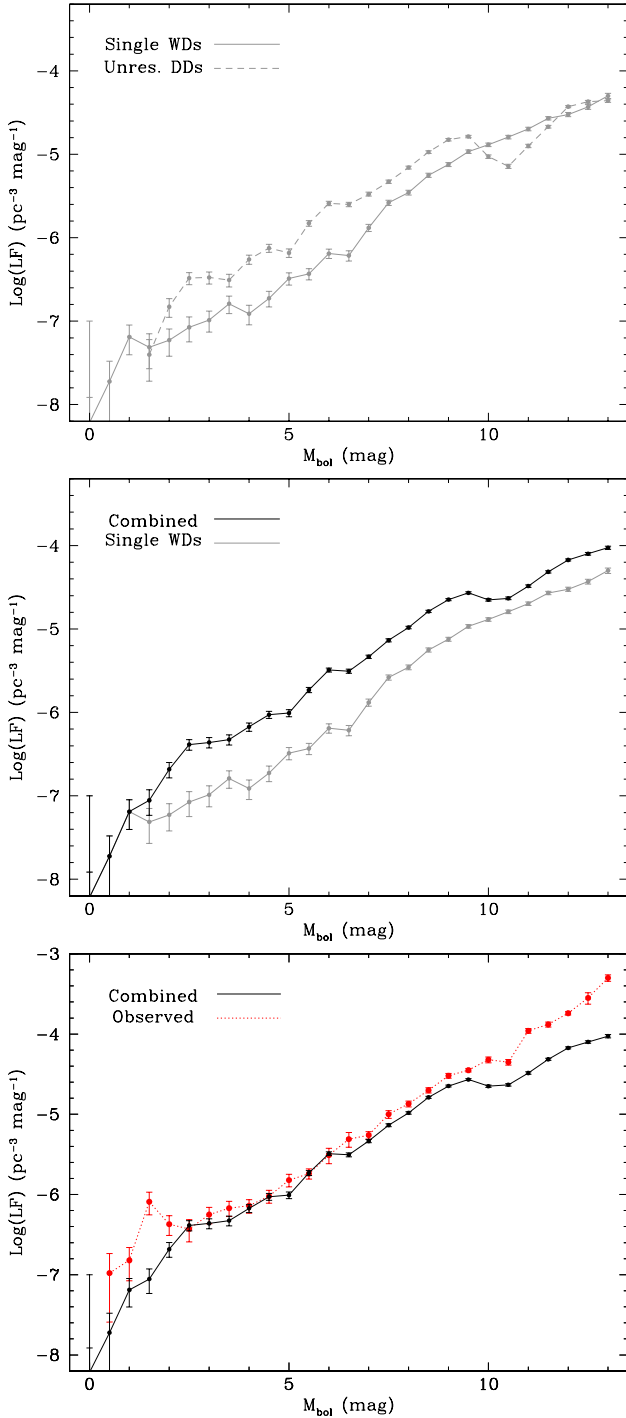


Figure 4. The same as Figure 1 but for the the model that produces the highest fraction of unresolved double degenerates.

in this case, the space density of single WDs was higher or similar to the one derived for unresolved WD binaries in most M_{bol} bins (see the top panel of Figure 5 and bottom panel of Figure 2). The effects of unresolved WD binaries are clearly noticeable at all bolometric magnitude bins except for $M_{\text{bol}} > 15$ mag (see the middle panel of Figure 5). This implies that even the highest contamination of unresolved double degenerates within the volume-limited *Gaia* sample is expected to have negligible effects on the implied

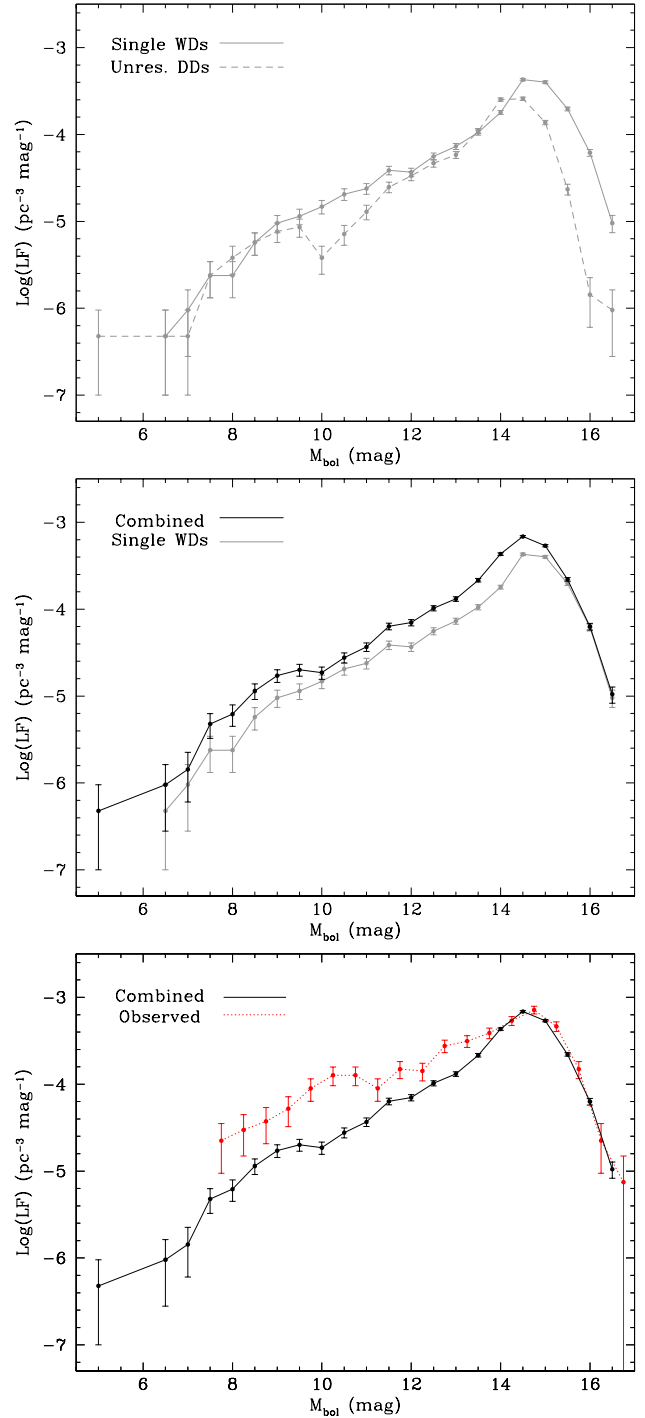


Figure 5. The same as Figure 3 but for the the model that produces the highest fraction of unresolved double degenerates.

age of the Galactic disc from the analysis of the cut-off of the WD luminosity function. However, this model implies contamination of unresolved double degenerates that *will* affect the derived star formation history, since these unresolved binaries would be considered as single WDs.

We conclude the adopted model in this section is most likely not realistic. However, the exercise performed here gives us an idea of the maximum contamination one can ex-

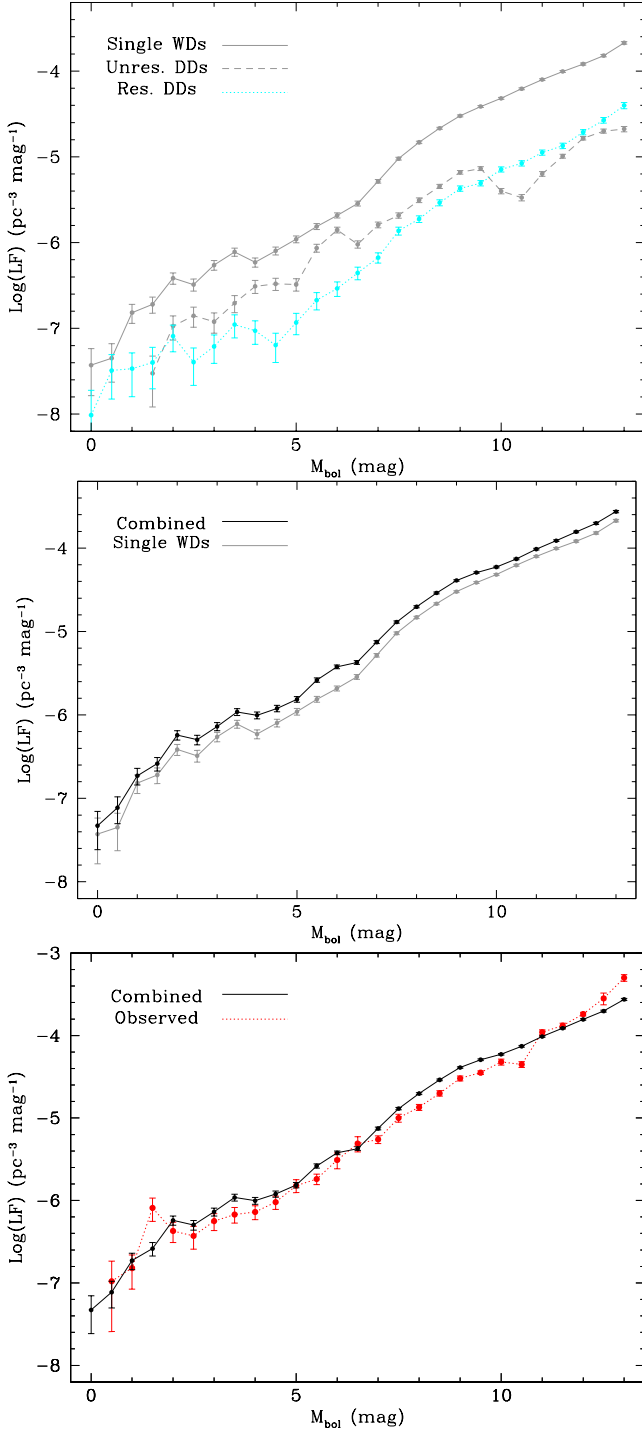


Figure 6. The same as Figure 1 but including the space density contribution from resolved double WDs (cyan dotted line in the top-right panel).

pect from unresolved double degenerates in both the SDSS and *Gaia* WD luminosity functions.

5.2 Resolved double degenerates

We followed the same procedures as outlined in Section 3 to derive the effect of resolved double WDs in the SDSS and *Gaia* luminosity functions. We emphasise that each binary

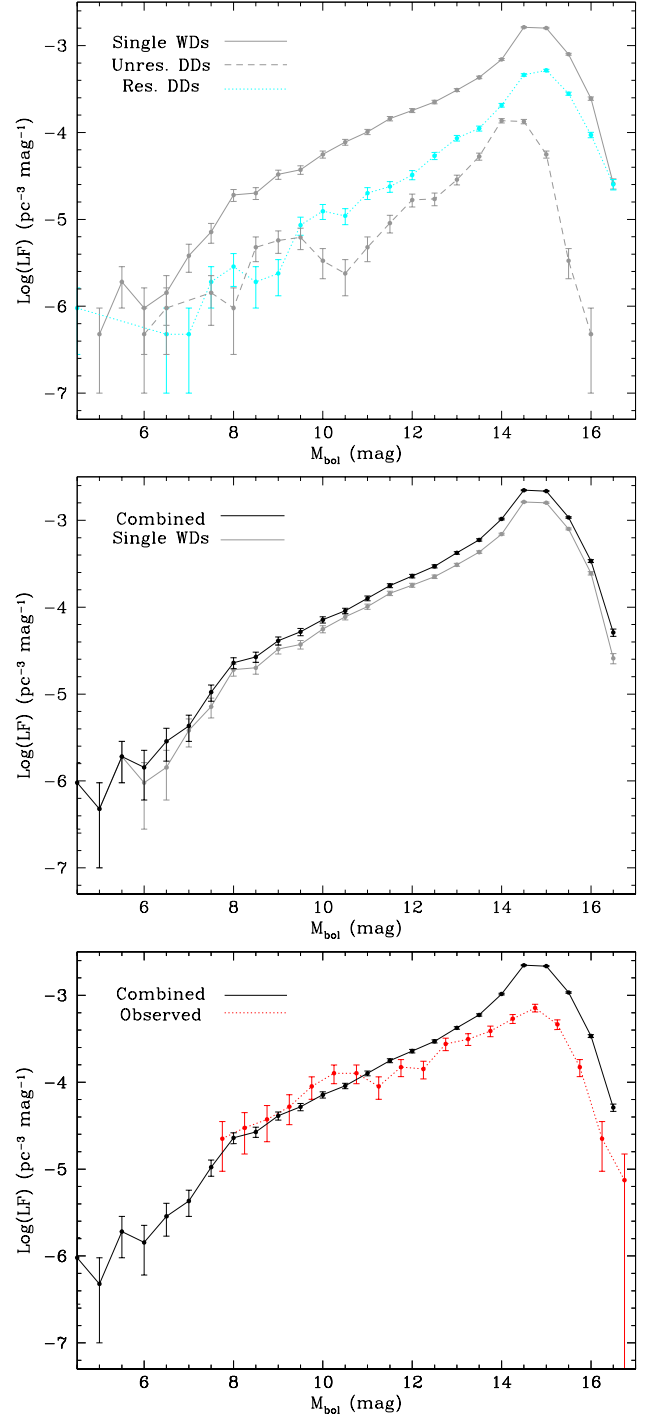


Figure 7. The same as Figure 3 but including the space density contribution from resolved double WDs (cyan dotted line in the top-right panel).

component was considered as a single WD which contributed in space density to the luminosity functions. The number of WDs in resolved double WDs in our synthetic samples that contributed to the luminosity functions were 2,817 for the SDSS sample³ and 4,090 for the *Gaia* sample. As expected,

³ As explained in Section 3, the SDSS synthetic samples are filtered according to a colour cut that defines the location of spec-

the number of resolved WDs in the *Gaia* sample was larger due to the better angular resolution (0.5" compared to 1" for SDSS) and smaller volume. The top panels of Figures 6 (SDSS) and 7 (*Gaia*) show the resolved double WD luminosity functions (cyan dotted lines) and the middle panels display the combined (single WDs plus unresolved and resolved double degenerates) functions. A comparison of the combined functions with the observed ones are provided in the bottom panels of the same figures.

Although the space densities increase due to the inclusion of resolved double degenerates in both samples, the shape of the combined synthetic luminosity functions are not too badly affected when compared to those derived from our standard model (see the middle and bottom panels of Figures 1 and 3). This implies the impact of resolved double degenerates in the WD luminosity function is low. In any case, it is important to emphasise that the binary components in resolved binaries can be easily identified if parallaxes and proper motions are available (see e.g. [El-Badry & Rix 2018](#) for the *Gaia* sample), which implies one can easily exclude these binaries from the observational analysis and thus avoid any possible contamination from such systems.

5.3 White dwarf plus main sequence binaries

In the present work we have only considered the double WD binary population and thus have excluded binaries consisting of a WD and a main sequence companion, i.e. WDMS binaries, which may contaminate the WD luminosity function too.

Unresolved WDMS binaries are generally easy to identify either from colours and/or spectra. Hence, these binaries will only contribute to the WD luminosity function if the MS companions are considerably less luminous than the WDs. That is, the colours and spectra of these systems are very similar to those of single WDs. For the 20 pc sample, [Toonen et al. \(2017\)](#) predicted, using the same models as here, ≈ 4 –8 unresolved double WDs as compared to ≈ 1 –2 unresolved WDMS binaries. For the majority of these WDMS binaries the flux was completely dominated by the main sequence companion, such that we would not confuse it for being a single WD. This is in line with the results obtained here, which indicate that the number of unresolved WDMS binaries in which the WD clearly dominates the flux emission is one order of magnitude lower than that of unresolved double degenerates. Hence, unresolved WDMS binaries clearly have no effect in altering the synthetic WD luminosity functions.

For the resolved WDMS binaries, the WDs can be considered to be part of the same population as that of single WDs. By adding those, the only noticeable effect would be to increase the space density of single WDs and to thus lower the fraction of double degenerates per bolometric magnitude bin. This would also correspond to an increase in space density implied by the combined luminosity function. However, as mentioned above, resolved binaries can easily

be identified using *Gaia* astrometric data and can hence be excluded from any observational analysis.

be identified using *Gaia* astrometric data and can hence be excluded from any observational analysis.

6 SUMMARY AND CONCLUSIONS

In this work we have studied the impact of unresolved double degenerates in the white dwarf luminosity function. To that end we have simulated the single and the double degenerate white dwarf populations in the solar neighbourhood using a population synthesis approach. The synthetic samples have been obtained using assumptions that best agree with the observational data, i.e. our standard model. Unresolved double white dwarfs have been analysed in the same way as if they were single point sources of fictitious effective temperatures, surface gravities and bolometric magnitudes. The synthetic luminosity functions have been obtained by considering the simulated samples as if they were observed by the SDSS magnitude-limited and *Gaia* volume-limited surveys.

Under the assumptions of our standard model we find that the effects of unresolved double degenerates in the white dwarf luminosity function are nearly negligible for the *Gaia* sample. Conversely, for the SDSS sample the contamination of unresolved double white dwarfs is significant at the brighter bins of the luminosity function ($M_{\text{bol}} < 6.5$ mag), reaching a maximum of $\approx 40\%$ of the total white dwarf population at $M_{\text{bol}} = 6$ mag. This implies that the age of the Galactic disc as well as the star formation history that will eventually be derived from the observed *Gaia* population are not expected to be affected by unresolved double degenerates. However, the star formation history derived from the SDSS sample, particularly during the most recent era, is expected to be affected to some extent (up to a 40% uncertainty) by the contamination of these binaries.

We have considered an additional model that maximizes the fraction of unresolved double degenerates, with the aim of evaluating the highest impact of such binaries in the SDSS and *Gaia* synthetic luminosity functions. Under the assumptions of this model, the number of double white dwarfs is twice that implied by our standard model. Consequently, the shape of the luminosity functions are severely affected and the star formation histories derived from both samples (SDSS and *Gaia*) would be strongly affected. However, even with the highest fraction of unresolved binaries considered, the age of the Galactic disc derived from the cut-off of the *Gaia* luminosity function is not expected to be affected. We also find that this model seems to be unrealistic, since the assumptions adopted are in poorer agreement with observations.

Finally, we evaluated the effects of resolved double degenerates as well as white dwarf plus main sequence binaries in the luminosity functions. Resolved binaries are found to slightly modify the shape of the luminosity functions. Nonetheless, these binaries can be easily identified observationally and thus excluded from the analysis. In the case of unresolved white dwarf-main sequence binaries, their impact on the white dwarf luminosity function is found to be negligible.

ACKNOWLEDGEMENTS

The authors are greatly indebted to D. Koester for developing the white dwarf mode atmosphere spectra used in this work. ARM acknowledges support from the MINECO under the Ramón y Cajal programme (RYC-2016-20254). ARM and S. Torres acknowledge support from the AYA2017-86274-P grant and the AGAUR grant SGR-661/2017. S. Toonen acknowledges support from the Netherlands Research Council NWO (grant VENI [nr. 639.041.645]).

REFERENCES

- Abt H. A., 1983, *ARA&A*, **21**, 343
 Alam S., et al., 2015, *ApJS*, **219**, 12
 Althaus L. G., Córscico A. H., Isern J., García-Berro E., 2010, *A&ARv*, **18**, 471
 Andrews J. J., Agüeros M. A., Gianninas A., Kilic M., Dhital S., Anderson S. F., 2015, *ApJ*, **815**, 63
 Anguiano B., Rebassa-Mansergas A., García-Berro E., Torres S., Freeman K. C., Zwitter T., 2017, *MNRAS*, **469**, 2102
 Blouin S., Dufour P., Thibeault C., Allard N. F., 2019, arXiv e-prints, p. [arXiv:1905.02174](https://arxiv.org/abs/1905.02174)
 Boissier S., Prantzos N., 1999, *MNRAS*, **307**, 857
 Boyle B. J., 1989, *MNRAS*, **240**, 533
 Camisassa M. E., Córscico A. H., Althaus L. G., Shibahashi H., 2016, *A&A*, **595**, A45
 Camisassa M. E., et al., 2018, arXiv e-prints, p. [arXiv:1807.03894](https://arxiv.org/abs/1807.03894)
 Claeys J. S. W., Pols O. R., Izzard R. G., Vink J., Verbunt F. W. M., 2014, *A&A*, **563**, A83
 Cojocaru R., Rebassa-Mansergas A., Torres S., García-Berro E., 2017, *MNRAS*, **470**, 1442
 Cummings J. D., Kalirai J. S., Tremblay P.-E., Ramirez-Ruiz E., Choi J., 2018, *ApJ*, **866**, 21
 Darwin G., 1879, *Phil. Trans. Roy. Soc.*, **170**, 447
 De Gennaro S., von Hippel T., Winget D. E., Kepler S. O., Nitta A., Koester D., Althaus L., 2008, *AJ*, **135**, 1
 De Gerónimo F. C., Camisassa M. E., Córscico A. H., Althaus L. G., 2018, arXiv e-prints, p. [arXiv:1809.09144](https://arxiv.org/abs/1809.09144)
 De Rosa R. J., et al., 2014, *MNRAS*, **437**, 1216
 Diaz-Pinto A., Garcia-Berro E., Hernanz M., Isern J., Mochkovitch R., 1994, *A&A*, **282**, 86
 Duchêne G., Kraus A., 2013, *ARA&A*, **51**, 269
 El-Badry K., Rix H.-W., 2018, *MNRAS*, **480**, 4884
 Fontaine G., Brassard P., Bergeron P., 2001, *pas*, **113**, 409
 Gaia Collaboration et al., 2016, *A&A*, **595**, A1
 García-Berro E., Oswalt T. D., 2016, *New Astron. Rev.*, **72**, 1
 Garcia-Berro E., Hernanz M., Isern J., Mochkovitch R., 1988, *Nature*, **333**, 642
 García-Berro E., et al., 2010, *Nature*, **465**, 194
 Gentile Fusillo N. P., et al., 2019, *MNRAS*, **482**, 4570
 Girven J., Gänsicke B. T., Steeghs D., Koester D., 2011, *MNRAS*, **417**, 1210
 Green R. F., 1980, *ApJ*, **238**, 685
 Hansen B. M. S., et al., 2013, *Nature*, **500**, 51
 Harris H. C., et al., 2006, *AJ*, **131**, 571
 Heggie D. C., 1975, *MNRAS*, **173**, 729
 Holberg J. B., Bergeron P., 2006, *AJ*, **132**, 1221
 Hollands M. A., Tremblay P. E., Gänsicke B. T., Gentile-Fusillo N. P., Toonen S., 2018, *MNRAS*, **480**, 3942
 Hu Q., Wu C., Wu X. B., 2007, *A&A*, **466**, 627
 Isern J., 2019, *ApJ*, **878**, L11
 Ivanova N., et al., 2013, *A&ARv*, **21**, 59
 Jeffery E. J., von Hippel T., DeGennaro S., van Dyk D. A., Stein N., Jefferys W. H., 2011, *ApJ*, **730**, 35
 Jiménez-Esteban F. M., Torres S., Rebassa-Mansergas A., Skrobogotov G., Solano E., Cantero C., Rodrigo C., 2018, *MNRAS*, **480**, 4505
 Kepler S. O., et al., 2019, *MNRAS*, **486**, 2169
 Kilic M., Munn J. A., Harris H. C., von Hippel T., Liebert J. W., Williams K. A., Jeffery E., DeGennaro S., 2017, *ApJ*, **837**, 162
 Kilic M., Hambly N. C., Bergeron P., Genest-Beaulieu C., Rowell N., 2018, *MNRAS*, **479**, L113
 Koester D., 2010, *Mem. Soc. Astron. Italiana*, **81**, 921
 Kowalski P. M., Saumon D., 2006, *ApJ*, **651**, L137
 Kroupa P., Tout C. A., Gilmore G., 1993, *MNRAS*, **262**, 545
 Krzesinski J., Kleinman S. J., Nitta A., Hügelmeier S., Dreizler S., Liebert J., Harris H., 2009, *A&A*, **508**, 339
 Limoges M. M., Bergeron P., Lépine S., 2015, *ApJS*, **219**, 19
 Livio M., Soker N., 1988, *ApJ*, **329**, 764
 Maoz D., Hallakoun N., Badenes C., 2018, *MNRAS*, **476**, 2584
 Moe M., Di Stefano R., 2017, *ApJS*, **230**, 15
 Nelemans G., Verbunt F., Yungelson L. R., Portegies Zwart S. F., 2000, *A&A*, **360**, 1011
 Nelemans G., Yungelson L. R., Portegies Zwart S. F., Verbunt F., 2001a, *A&A*, **365**, 491
 Nelemans G., Yungelson L. R., Portegies Zwart S. F., Verbunt F., 2001b, *A&A*, **365**, 491
 Paczynski B., 1976, in P. Eggleton, S. Mitton, & J. Whelan ed., *IAU Symposium Vol. 73, Structure and Evolution of Close Binary Systems*. Kluwer, Dordrecht, p. 75
 Pietrinferni A., Cassisi S., Salaris M., Castelli F., 2004, *ApJ*, **612**, 168
 Portegies Zwart S. F., Verbunt F., 1996, *A&A*, **309**, 179
 Raghavan D., et al., 2010, *ApJS*, **190**, 1
 Rebassa-Mansergas A., Schreiber M. R., Gänsicke B. T., 2013, *MNRAS*, **429**, 3570
 Rebassa-Mansergas A., et al., 2015a, *MNRAS*, **450**, 743
 Rebassa-Mansergas A., Rybicka M., Liu X. W., Han Z., García-Berro E., 2015b, *MNRAS*, **452**, 1637
 Rebassa-Mansergas A., et al., 2016, *MNRAS*, **463**, 1137
 Rebassa-Mansergas A., Parsons S. G., García-Berro E., Gänsicke B. T., Schreiber M. R., Rybicka M., Koester D., 2017, *MNRAS*, **466**, 1575
 Rebassa-Mansergas A., Toonen S., Korol V., Torres S., 2019, *MNRAS*, **482**, 3656
 Renedo I., Althaus L. G., Miller Bertolami M. M., Romero A. D., Córscico A. H., Rohrmann R. D., García-Berro E., 2010, *ApJ*, **717**, 183
 Rowell N., 2013, *MNRAS*, **434**, 1549
 SDSS-III Collaboration et al., 2012, preprint, ([arXiv:1207.7137](https://arxiv.org/abs/1207.7137))
 Schmidt M., 1968, *ApJ*, **151**, 393
 Siess L., 2007, *A&A*, **476**, 893
 Skinner J. N., Morgan D. P., West A. A., Lépine S., Thorstensen J. R., 2017, *AJ*, **154**, 118
 Stoughton C., et al., 2002, *AJ*, **123**, 485
 Temmink K. D., Toonen S., Zapartas E., Justham S., Gänsicke B. T., 2019, arXiv e-prints, p. [arXiv:1910.05335](https://arxiv.org/abs/1910.05335)
 Tononi J., Torres S., García-Berro E., Camisassa M. E., Althaus L. G., Rebassa-Mansergas A., 2019, *A&A*, **628**, A52
 Toonen S., Nelemans G., 2013, *A&A*, **557**, A87
 Toonen S., Nelemans G., Portegies Zwart S., 2012, *A&A*, **546**, A70
 Toonen S., Claeys J. S. W., Mennekens N., Ruiter A. J., 2014, *A&A*, **562**, A14
 Toonen S., Hollands M., Gänsicke B. T., Boekholt T., 2017, *A&A*, **602**, A16
 Torres S., García-Berro E., 2016, *A&A*, **588**, A35
 Torres S., García-Berro E., Krzesinski J., Kleinman S. J., 2014, *A&A*, **563**, A47
 Torres S., García-Berro E., Althaus L. G., Camisassa M. E., 2015, *A&A*, **581**, A90

- Torres S., Cantero C., Rebassa-Mansergas A., Skorobogatov G., Jiménez-Esteban F. M., Solano E., 2019a, *MNRAS*, **485**, 5573
- Torres S., Cantero C., Camisassa M. E., Antoja T., Rebassa-Mansergas A., Althaus L. r. G., Thelemaque T., Cánovas H., 2019b, *A&A*, **629**, L6
- Tremblay P. E., Bergeron P., Gianninas A., 2011, *ApJ*, **730**, 128
- Tremblay P.-E., et al., 2019, *Nature*, **565**, 202
- Tutukov A., Yungelson L., 1979, in Conti P. S., De Loore C. W. H., eds, IAU Symposium Vol. 83, Mass Loss and Evolution of O-Type Stars. pp 401–406
- Webbink R. F., 1984, *ApJ*, **277**, 355
- Winget D. E., Hansen C. J., Liebert J., van Horn H. M., Fontaine G., Nather R. E., Kepler S. O., Lamb D. Q., 1987, *apjl*, 315, L77
- Yanny B., et al., 2009, *AJ*, **137**, 4377
- York D. G., et al., 2000, *AJ*, **120**, 1579
- de Bruijne J. H. J., Allen M., Azaz S., Krone-Martins A., Prod'homme T., Hestroffer D., 2015, *A&A*, **576**, A74

This paper has been typeset from a $\text{\TeX}/\text{\LaTeX}$ file prepared by the author.